COMMUNICATIONS IN SCIENCE AND TECHNOLOGY
Homepage: cst.kipmi.or.id

Tuning the magnetic states in AA-stacked bilayer zigzag graphene nanoribbons

Teguh Budi Prayitno*

Physics Department, Faculty of Mathematics and Natural Science, Universitas Negeri Jakarta, East Jakarta 13220, Indonesia

Article history:
Received: 23 May 2022 / Received in revised form: 20 June 2022 / Accepted: 21 June 2022

Abstract

Available reports mentioned that the magnetic ground state in the AA-stacked bilayer zigzag graphene nanoribbons is the non-magnetic state. As a consequence, it is impossible to exploit magnetism for future electronic devices. This paper aims to show how to generate magnetism in the AA-stacked bilayer zigzag graphene nanoribbons by employing first-principles calculations. As we stacked different ribbon widths, the magnetic ground states appeared for all the thicknesses. In general, the G-type antiferromagnetic state, which is the antiferromagnetic alignment between both intraplane- and interplane-edge carbon atoms, is the ground state for all the thicknesses. We also found that the degenerate magnetic ground states and excited states may appear under certain thicknesses, thus yielding the richness of the magnetic state. As hole-electron doping was applied, a phase transition of magnetic ground state emerged for certain thicknesses, indicating that a new magnetic ground state in the AA-stacked bilayer zigzag graphene nanoribbons can be tuned by the doping.

Keywords: Graphene nanoribbon; magnetic state; phase transition

1. Introduction

Investigations on the electronic and magnetic features in the low-dimensional materials have exhibited a number of significant impacts on the condensed matter physics after graphene has been discovered as a two-dimensional hexagonal carbon lattice [1-3]. Certainly, for being a highly prominent candidate for future devices in spintronics and nanoelectronics, graphene becomes a concern [4, 5].To exploit the electronic or magnetic properties of this material, recognition of its edge structures in the microscopic scale is deemed necessary. Previously, Fujita et al. showed that graphene nanoribbon (GNR), a one-dimensional structure of graphene, possesses extraordinary properties induced by the carbon edges [6, 7]. Recently, several experiments have been realized to grow the GNR by some methods [8-10]. Later, theoretical explorations on the electronic and magnetic properties in the GNR are employed in such a way by applying the electric field [12-14] or doping [15-17] to seek applicable devices.

Based on the fundamental shape, the GNR is classified into two: the zigzag GNR (ZGNR) and armchair GNR (AGNR). It has been well-known that the ground state of ZGNR is an antiferromagnetic (AFM) state [6], while the AGNR has a non-magnetic state [18]. Thus, the magnetic features in the ZGNR are more exploited than those in the AGNR. Arranging the spin orientations of carbon atoms at the edges in the ZGNR is necessary to determine the ground state. Even though the ground state of ZGNR is well-known as an AFM state, other configurations such as ferromagnetic (FM) state or spiral state can be useful for some electronic devices. As for an AFM ground state, it can be used to discuss the spin-waves excitation to predict the spin stiffness or critical temperature [19-22]. Those two properties are very useful to design spintronic devices, which will work at room temperature. At the same time, the FM state can induce a metallic state [23], while the spiral state can be utilized to construct a domain wall [24]. Note that the spiral state can be induced by incorporating a metal atom [25, 26] or taking the electric field into account [27].

There are two types of stacked bilayer ZGNR, namely the AA- and AB-stacked bilayer ZGNRs. These bilayer structures have been successfully produced by available methods [28-30], possess the band gap by applying the electric field [31, 32] or constructing the edge alignments [33], and are robust to the external perturbations [34]. For this, they are also prominent in the development of carbon-based spintronic devices, such as for the spin transport [35, 36]. Due to the binding energy in graphene, the AB-stacked bilayer structure is more stable than the AA-stacked bilayer one [37, 38]. However, from the magnetic perspective, the AA-stacked bilayer ZGNR is more energetically stable than the AB-stacked one. This is because the AA-stacked bilayer ZGNR displays the non-magnetic state, while the AB- stacked one shows the spin-polarized state [39]. For this reason, the consideration of magnetism in the AA-stacked bilayer ZGNR is not completely explored.

Similar to the monolayer case, the magnetic ground state of bilayer ZGNR is determined by the alignments of magnetic

* Corresponding author.
Email: teguh-budi@unj.ac.id
https://doi.org/10.21924/cst.7.1.2022.823

carbon atoms at the edges. The ground state, therefore, will also be controlled by the interplane and intraplane edge orders, giving the different magnetic stability. In this paper, we investigated the magnetic ground state of AA-stacked bilayer ZGNR for five magnetic configurations as performed by Sawada et al. [40]. Previously, they showed that, of five magnetic configurations in the AB-stacked bilayer ZGNR for all thicknesses, there was only one magnetic ground state, namely, the C-type antiferromagnetic state, which had the interplane FM and intraplane AFM edge configurations. This suggests that the magnetic ground state is robust to the thickness.

As performing the same treatment above, on the contrary, we obtained the magnetic ground states, which were dependent upon certain conditions in the AA-stacked bilayer ZGNR. When we stacked two ZGNRs with different ribbon widths, we observed the degenerate magnetic ground states and excited states, which depended on the thickness. Also, there was only one state which always became a magnetic ground state for all thicknesses, namely, the G-type antiferromagnetic state which had the interplane AFM and intraplane AFM edge configurations. This magnetic ground state also emerged as hole-electron doping was considered, but then it was replaced by other magnetic ground states at certain conditions. This yielded phase transitions in the AA-stacked bilayer ZGNR under the doping. This means that controlling the magnetic state in the AA-stacked bilayer ZGNR can be realized by using the doping.

2. Materials and Methods

For the investigation, a one-dimensional slab model of AA-stacked hydrogen passivated bilayer ZGNR was constructed with the experimental lattice parameter of graphite (2.46 Å) along *x*-axis (periodic direction) as shown in figure 1(a). We constructed two structure models in which we fixed the 10 dimers at the bottom and varied the number of dimers at the top, as shown in figures 1(b-c). Here, the number of dimers was related to the ribbon width. To encounter the interaction in the non-periodic directions (*y*- and *z*- axes), we set 30 Å to generate a vacuum region. We also varied the thicknesses *d* to see the appearances of magnetic states.

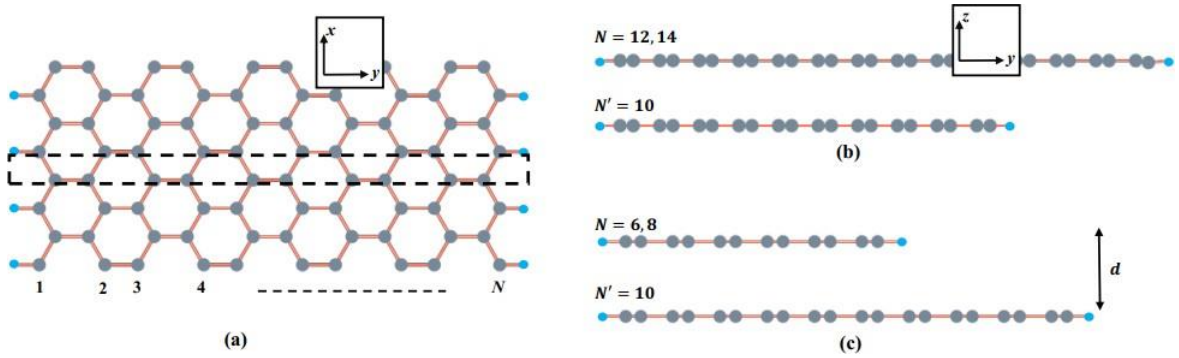

Fig. 1. Crystal structure of AA-stacked bilayer ZGNR from top view (a) and side view (b, c). Here, the dashed square and *d* are addressed to the unit cell and thickness

We carried out the first-principles calculations by using the OpenMX package [41] within the density functional theory. This package employed the localized basis orbitals [42] and norm-conserving pseudopotentials according to Troullier and Martins [43]. To obtain the converged results with good accuracy, we set the basis orbitals of s_2p_2 and s_2p_1 for the carbon and hydrogen atoms, respectively. Here, s and p are the valence and polarization orbitals generated numerically by the confinement method [42]. We also employed the generalized gradient approximation (GGA) in accordance with Perdew, Burke, and Ernzerhof [44] for treating the electron-electron interaction. In these self-consistent calculations, we also set a k-point sampling of $62 \times 1 \times 1$ and a cutoff energy of 250 Ry. Before running the calculations, we performed the optimized atomic positions on *x* and *y* planes at which the forces act on atoms were less than 0.0001 Hartree/Bohr and fixed the thickness *d*.

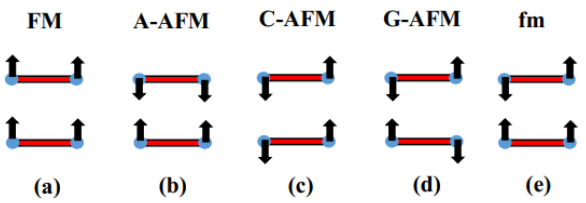

Fig. 2. Five different collinear magnetic configurations at theedges, namely, the FM (a), A-AFM (b), C-AFM (c), G-AFM (d), and fm (e) states

Since the magnetic order induced by the edges has many possible configurations, we focused on the five collinear magnetic alignments, as shown in figure 2. These configurations are based on the previous work of Sawada et al. [40], who considered the interplane and intraplane edges. For the AFM configurations, the A-AFM was constructed by the interplane AFM and intraplane FM edges, the C-AFM was built by the interplane FM and intraplane AFM edges, while the G-AFM was established by the interplane AFM and intraplane AFM edges. Meanwhile, the ferrimagnetic (fm) state was constructed by a combination of FM/AFM at the interplane/intraplane edges, as shown in figure 2(e).

3. Results and Discussions

To start the discussion, we considered the experimental thickness $d = 3.35$ Å for all the ribbon widths *N*. Figure 3 displays the energy dispersions for the magnetic configurations of bilayer *N*-ZGNR. We observed that the FM, C-AFM, and fm states exhibited the metallic state while the A-AFM and G-AFM states showed the insulating state. It was also found that all the configurations became the magnetic states where the A-AFM and G-AFM states together became the magnetic ground states, in opposite to the AB-stacked bilayer ZGNR [40]. Furthermore,we found that all the AFM states in the AB-stacked structure always exhibited the insulating state

while the AFM-state, in the case of C-AFM state, in the AA-stacked structure may exhibit the metallic state, as shown in figure 3.

For discussing other thicknesses *d*, we fixed the atomic positions on *x* and *y* planes and only changed *d*. As we varied *d*, we found interesting tendencies, as shown in figure 4. First of all, the G-AFM state became the magnetic ground state for all *d* and *N*, suggesting that the G-AFM ground state is robust under *d* and *N*. At the same time, the A-AFM state together with the G-AFM state became the magnetic ground states in the interval of 2.85 Å $\leq d \leq$ 3.35 Å for all *N*, showing the degenerate magnetic ground states. Here, the G-AFM state was the only magneticground state at $d = 2.35$ Åand $d > 3.35$ Å. In addition, we observed that some magnetic excited states became degenerate, such as the FM, C-AFM, and fm states that had the same energy in the interval of 2.35 Å $\leq d \leq$ 3.35 Å for $N = 6, 8, 12, 14$. The details can be found in table 1. As seen in table 1, the magnetic ground state always possessed the largest energy gap among all the states, similar to the monolayer and AB-stacked bilayer cases.

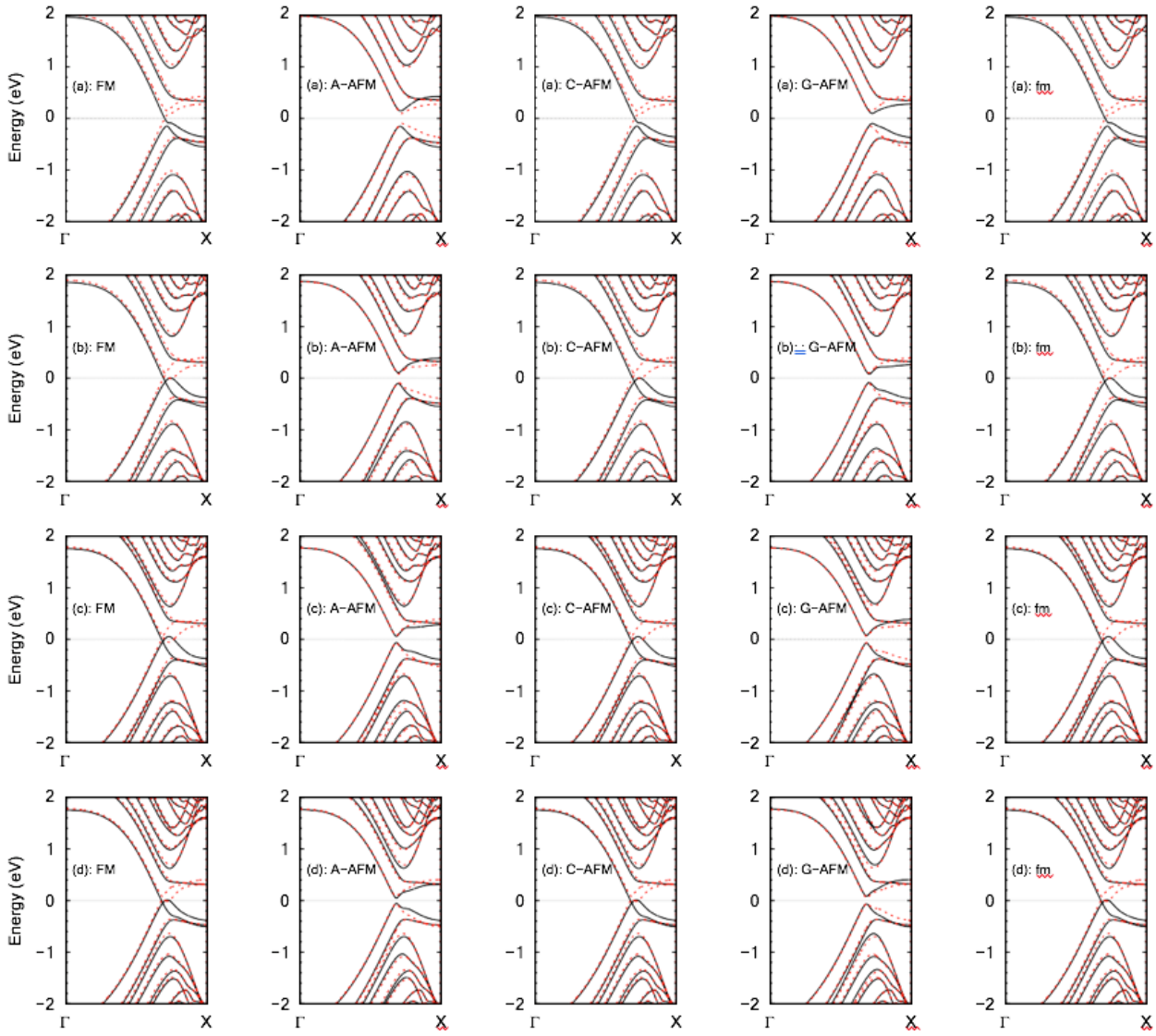

Fig. 3. Energy dispersion relations of bilayer 6-ZGNR (a), 8-ZGNR (b), 12-ZGNR (c), 14-ZGNR (d) at thickness $d = 3.35$ Å. The Fermi energy $E_F = 0$ is shown by the horizontal dashed line. Meanwhile, the states of spin up and spin down are representedby the solid and dashed lines, respectively

Regarding the magnetic moment, the clear difference between small *d* and large *d* can be found in table 1. At the small *d*, even the localized edge state occurred, the bonding between edge carbon atoms along the interplane-edge direction were sufficiently strong, thus resisting the spin polarization. Consequently, this led to the small magnetic moments at the edges. Contrarily, as we increased *d*, the bonding between layers became weak; thus in this condition the localized edge states overcame the bonding between edge carbon atoms along the interplane-edge direction, appearing the spin polarization. In this moment the large magnetic moments at the edges occurred then. It can be assumed that the magnetism in the AA-stacked bilayer ZGNR can be strengthened by increasing *d*, thus reducing the bonding between edge carbon atoms along the interplane-edge direction.

For the general notes, we assumed that the G-AFM ground state was independent with the *N* and *d* in the AA-stacked bilayer ZGNR, which differed from the AB-stacked structure [40].This meant that the AFM coupling (FM coupling) at the interplane edge atoms dominated the magnetism in the AA-stacked (AB-stacked) bilayer ZGNR. This result is also consistent with the previous works of Lee et al. by different approaches [45, 46]. Note that the G-AFM ground state also emerges in the AB-stacked bilayer ZGNR for the non-collinear structure [47].

Table 1. Computed total energy difference ΔE (meV), energy gap E_g (eV), and averaged magnetic moment of four edge carbon atoms M (μB/atom) of N-ZGNR under several configurations and thicknesses d. Here, the total energy difference ΔE is calculated with respect to the ground state. The boxes refer to the ground states

N	State	d = 2.35 Å			d = 2.85 Å			d = 3.35 Å			d = 3.85 Å			d = 4.35 Å		
		ΔE	E_g	M	ΔE	E_g	M	ΔE	E_g	M	ΔE	E_g	M	ΔE	E_g	M
6	FM	19.37	0.0	0.17	10.21	0.0	0.14	3.99	0.0	0.20	32.50	0.0	0.20	19.88	0.0	0.31
	A-AFM	41.17	0.0	0.08	0.0	0.12	0.16	0.0	0.20	0.22	14.95	0.0	0.22	15.80	0.0	0.31
	C-AFM	19.37	0.0	0.17	10.21	0.0	0.14	3.99	0.0	0.20	20.74	0.23	0.19	4.69	0.30	0.32
	G-AFM	0.0	0.20	0.19	0.0	0.12	0.16	0.0	0.20	0.22	0.0	0.30	0.22	0.0	0.32	0.32
	fm	19.37	0.0	0.17	10.21	0.0	0.14	3.99	0.0	0.20	5.62	0.0	0.20	5.83	0.0	0.32
8	FM	53.95	0.0	0.07	13.58	0.0	0.12	14.11	0.0	0.17	30.98	0.0	0.32	17.05	0.0	0.32
	A-AFM	53.95	0.0	0.07	0.0	0.08	0.13	0.0	0.16	0.21	11.62	0.0	0.30	12.45	0.0	0.31
	C-AFM	53.95	0.0	0.07	13.58	0.0	0.12	14.11	0.0	0.17	23.74	0.16	0.33	5.10	0.30	0.33
	G-AFM	0.0	0.20	0.16	0.0	0.08	0.13	0.0	0.16	0.21	0.0	0.29	0.31	0.0	0.32	0.32
	fm	30.30	0.0	0.11	13.58	0.0	0.12	14.11	0.0	0.17	6.42	0.0	0.31	5.98	0.0	0.32
12	FM	65.35	0.0	0.08	13.14	0.0	0.12	13.85	0.0	0.16	29.57	0.0	0.32	13.75	0.0	0.32
	A-AFM	65.35	0.0	0.08	0.0	0.07	0.13	0.0	0.12	0.19	8.29	0.06	0.30	9.69	0.0	0.32
	C-AFM	65.35	0.0	0.08	13.14	0.0	0.12	13.85	0.0	0.16	25.85	0.16	0.33	5.39	0.25	0.33
	G-AFM	0.0	0.17	0.18	0.0	0.07	0.13	0.0	0.12	0.19	0.0	0.25	0.31	0.0	0.29	0.33
	fm	65.35	0.0	0.08	13.14	0.0	0.12	13.85	0.0	0.16	7.0	0.0	0.31	6.12	0.0	0.32
14	FM	66.47	0.0	0.09	5.88	0.0	0.14	7.41	0.0	0.17	28.34	0.0	0.32	12.82	0.0	0.32
	A-AFM	66.47	0.0	0.09	0.0	0.06	0.15	0.0	0.11	0.19	7.48	0.03	0.30	8.47	0.0	0.32
	C-AFM	66.47	0.0	0.09	5.88	0.0	0.14	7.41	0.0	0.17	24.64	0.08	0.33	5.26	0.22	0.33
	G-AFM	0.0	0.18	0.19	0.0	0.06	0.15	0.0	0.11	0.19	0.0	0.22	0.31	0.0	0.25	0.33
	fm	66.47	0.0	0.09	5.88	0.0	0.14	7.41	0.0	0.17	5.95	0.0	0.31	6.02	0.0	0.32

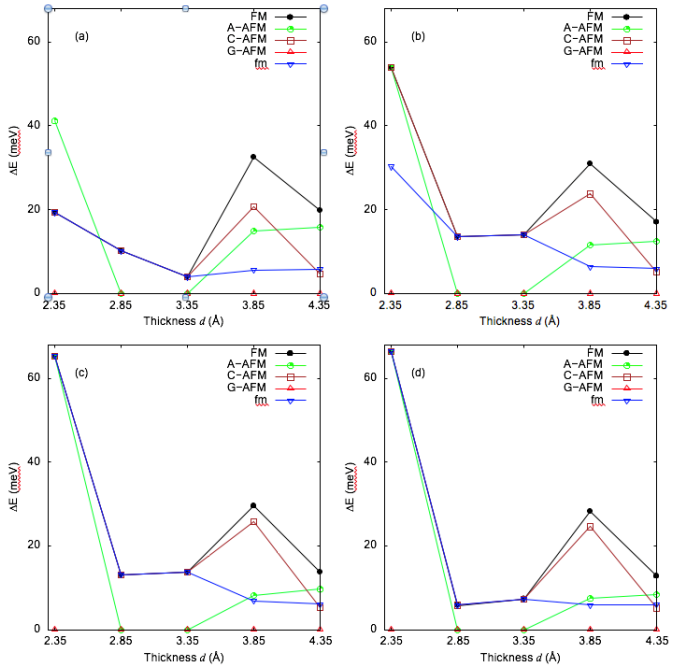

Fig. 4. Total energy difference ΔE with respect to the ground state of bilayer 6-ZGNR (a), 8-ZGNR (b), 12-ZGNR (c), and14-ZGNR (d) as a function of thickness d

Next, we considered the carrier-doped bilayer ZGNR by introducing hole-electron doping. To do so, we applied the Fermi level shift approach as we gave a homogeneous background charge as if the system remained neutral [48,49]. The realization of this doping can be performed experimentally by using the chemical doping [48]. We specified the number of carrier doping per cell as x (e/cell). Here, hole (electron) doping was expressed by the positive (negative) e values. We only considered d = 2.35 Å, 3.35 Å and 4.35 Å for N = 6 and 14. We then computed the total energy difference ΔE with respect to the ground state as a function of x. At d = 2.35 Å as shown in figure 5, the G-AFM state became the ground state for all the doping and ribbon widths, indicating that, in this case, the G-AFM state was robust to the doping and ribbon widths. Meanwhile, the excited states became degenerate under N. For N = 6 except for the A-AFM state, the FM, C-AFM, and fm states became degenerate, as displayed in figure 5(a). Contrarily, all the excited states became degenerate for N = 14, as displayed in figure 5(b). These results implied that there was no magnetic phase transition at d = 2.35 Å for all N.

At d = 3.35 Å in figure 6, we observed different tendencies as the previous one. For N = 6, the A-AFM and G-AFM states became the degenerate magnetic ground states in the interval of -0.06 e/cell ≤ x ≤ 0.06 e/cell. Meanwhile, the FM, C-AFM and fm states became the degenerate magnetic ground states in the interval of x < -0.06 e/cell and x > 0.06 e/cell, leading to the magnetic phase transition, as shown in figure 6(a). Meanwhile, as for N = 14 in figure 6(b), the A-AFM and G-AFM states became the degenerate magnetic ground states for all doping, thus also indicating no magnetic phase transition.

At d = 4.35 Å in figure 7, we observed the magnetic phase transition for all N. For N = 6, the G-AFM state became the magnetic ground state in the interval of -0.02 e/cell ≤ x ≤ 0.02 e/cell. While, the fm state became the magnetic ground state in the interval of x < -0.02 e/cell and x > 0.02 e/cell, leading to the magnetic phase transition, as shown in figure 7(a). Meanwhile, as for N = 14 in figure 7(b), the G-AFM state became the magnetic ground state in the interval of -0.06 e/cell≤ x ≤0.02 e/cell. Then, the fm state became the magnetic ground state in the interval of 0.04 e/cell≤ x ≤0.06 e/cell. The A-AFM state, furthermore, became the magnetic ground state in the interval of x < -0.06 e/cell and x > 0.06 e/cell, also undergoing to the magnetic phase transition.

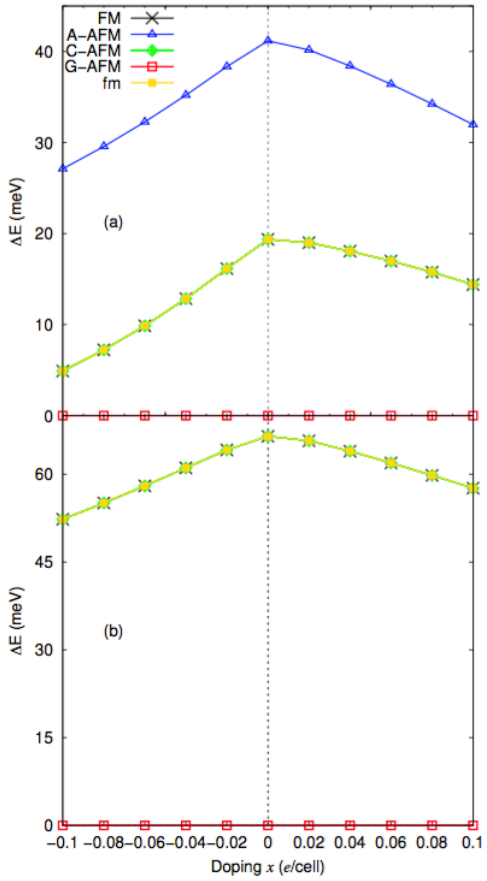

Fig. 5. Total energy difference ΔE with respect to the ground state of bilayer 6-ZGNR (a) and 14-ZGNR (b) at thickness d = 2.35 Å as a function of doping x

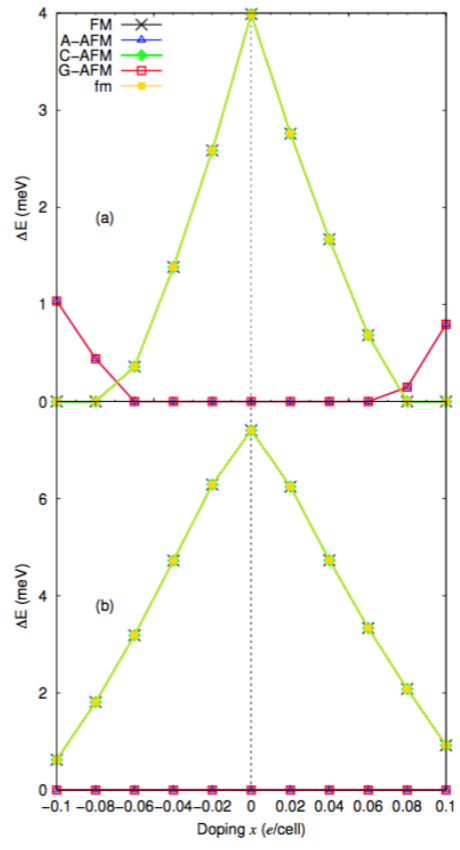

Fig. 6. Total energy difference ΔE with respect to the ground state of bilayer 6-ZGNR (a) and 14-ZGNR (b) at thickness d = 3.35 Å as a function of doping x

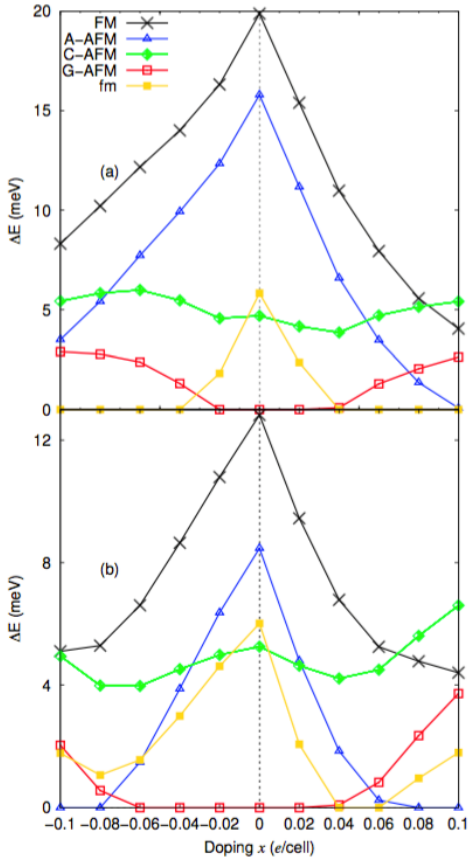

Fig. 7. Total energy difference ΔE with respect to the ground state of bilayer 6-ZGNR (a) and 14-ZGNR (b) at thickness d = 4.35 Å as a function of doping x

In the bilayer ZGNR, the physical properties were determined by the magnetic couplings at the intraplane- and interplane-edge atoms. At d = 2.35 Å in figure 5, since the G- AFM state was only the magnetic ground state for all the doping and N, the AFM couplings at both the intraplane and interplane- edge atoms maintain as $|x|$ increased. Thus, we expected that both the intraplane and interplane AFM couplings remained unchanged under the carrier doping caused by the lattice defects or impurities in the AA-stacked bilayer N-ZGNR. Moreover, although the FM, A-AFM, C-AFM, and fm states were the different magnetic excited states, they had the same FM coupling at the interplane-edge atoms except for the A-AFM state. This implies that the interplane FM coupling will be never found as the most stable state under the doping.

At d = 3.35Å, in the case of N = 6 in figure 6 (a) it can be seen that at $|x| \leq 0.06$ e/cell, the AFM coupling held at the interplane-edge atoms while either the FM coupling (A-AFM state) or the AFM coupling (G-AFM state) at the intraplane-edge atoms was maintained. Except for the fm state, the AFM coupling was then replaced by the FM coupling at the interplane-edge atoms while either the FM coupling (FM state) or the AFM coupling (C-AFM state) at the intraplane-edge atoms wa sstill maintained as $|x|$ increased. This indicates that the stability of the interplane FM ordering only works at high x, which is the same result as in the AB-stacked case [50]. As for N = 14 in figure 6 (b), a similar behavior occurred as in the case of N = 6 but for all the doping, i.e., the A-AFM and G-AFM states were the magnetic ground states.This indicates that the interplane AFM ordering is robust under the doping.

At d = 4.35 Å it can also be seen that the magnetic ground

state was still dominated by the interplane AFM ordering, but no degenerate magnetic state appeared for all N in both the ground state and excited state. From these results, we expected that the degenerate magnetic states sensitively depended on the thickness. As the thickness increased, the bonding between interplane-edge carbon atoms was weakened; thus the magnetism was maintained. However, a consequence corresponds to the unavailable degenerate magnetic states for both the magnetic ground state and excited states.

4. Conclusion

We investigated the magnetic ground states of AA-stacked bilayer ZGNR and found the degenerate magnetic ground states, dependent upon the ribbon width and thickness. We observed that the magnetic ground state was degenerate for certain thickness and became non-degenerate as the thickness increased. In general, the G-AFM state also became the magnetic ground state, which is robust to the ribbon width and thickness.

As hole-electron doping was introduced, the magnetic phase transitions generally occurred for all N at the high d, for example at $d = 4.35$ Å as we plotted the total energy difference with respect to the doping. However, no degeneracy appeared in both the magnetic ground state and excited state. When the thickness decreased, no magnetic phase transition appeared except for $N = 6$ at $d = 3.35$ Å. On the contrary, the degenerate magnetic states appeared. Unlike the AB-stacked bilayer ZGNR where there was no degenerate magnetic state, the degeneration in the AA-stacked form appeared due to the bonding between interplane-edge carbon atoms. In addition, this bonding governed the state in ZGNR to become magnetic or non-magnetic.

References

1. K. S. Novoselov, A. K. Geim, S. V. Morozov, D. Jiang, Y. Zhang, S. V. Dubonos, et al., *Electric field effect in atomically thin carbon films*, Science 306 (2004) 666-669.
2. K. S. Novoselov, A. K. Geim, S. V. Morozov, D. Jiang, M. I. Katsnelson, I. V. Grigorieva, et al., *Two-dimensional gas of massless Dirac fermions in graphene*, Nature 438 (2005) 197-200.
3. A. K. Geim and K. S. Novoselov, *The rise of graphene*, Nature Mater. 6 (2007) 183-191.
4. L. Liao, Y.-C. Lin, M. Bao, R. Cheng, J. Bai, Y. Liu, et al., *High-speed graphene transistors with a self-aligned nanowire gate*, Nature 467 (2010) 305-308.
5. F. Schwierz, *Graphene transistors*, Nat. Nanotech. 5 (2010) 487-496.
6. M. Fujita, K. Wakabayashi, K. Nakada and K. Kusakabe, *Peculiar localized state at zigzag graphite edge*, J. Phys. Soc. Jpn. 65 (1996) 1920-1923.
7. K. Nakada, M. Fujita, G. Dresselhaus and M. S. Dresselhaus, *Edge state in graphene ribbons: Nanometer size effect and edge shape dependence*, Phys.Rev. B 54 (1996) 17954-17961.
8. D. V. Kosynkin, A. L. Higginbotham, A. Sinitskii, J. R. Lomeda, A. Dimiev, B. K. Price, et al., *Longitudinal unzipping of carbon nanotubes to form graphene nanoribbons*, Nature 458 (2009) 872-876.
9. G. Z. Magda, X. Jin, I. Hagymási, P. Vancsó, Z. Osváth, P. Nemes-Incze, et al., *Room-temperature magnetic order on zigzag edges of narrow graphene nanoribbons*, Nature 514 (2014) 608-611.
10. P. Ruffieux, S. Wang, B. Yang, C. Sánchez-Sánchez, J. Liu, T. Dienel, et al., *On surface synthesis of graphene nanoribbons with zigzag edge topology*, Nature 531 (2016) 489–492.
11. S. Kawai, S. Nakatsuka, T. Hatakeyama, R. Pawlak, T. Meier, J. Tracey, et al., *Multiple heteroatom substitution to graphene nanoribbon*, Sci. Adv. 4 (2018) eaar7181.
12. Y.-W Son, M. L. Cohen and S. G. Louie, *Half-metallic graphene nanoribbons*, Nature 444 (2006) 347-349.
13. E. Rudberg, P. Sałek and Y. Luo, *Nonlocal exchange interaction removes half-metallicity in graphene nanoribbons*, Nano Lett. 7 (2007) 2211.
14. E.-J. Kan, Z. Li, J. Yang and J. G. Hou, *Will zigzag graphene nanoribbon turn to half metal under electric field?*, Appl. Phys. Lett. 91 (2007) 243116.
15. N. Gorjizadeh, A. A. Farajian, K. Esfarjani and Y. Kawazoe, *Spin and band-gap engineering in doped graphene nanoribbons*, Phys. Rev. B 78 (2008) 155427.
16. Z. Wang, *Alignment of graphene nanoribbons by an electric field*, Carbon 47 (2009) 3050-3053.
17. B. Mandal, S. Sarkar, A. Pramanik and P. Sarkar, *Doped defective graphene nanoribbons: a new class of materials with novel spin filtering properties*, RSC Adv. 4 (2014) 49946-49952.
18. S. Okada, *Energetics of nanoscale graphene ribbons: Edge geometries and electronic structures*, Phys. Rev. B 77 (2008) 041408(R).
19. O. V. Yazyev and M. I. Katsnelson, *Magnetic correlations at graphene edges: basis for novel spintronics devices*, Phys. Rev. Lett. 100 (2008) 047209.
20. J.-W. Rhim and K. Moon, *Spin stiffness of graphene and zigzag graphene nanoribbons*, Phys. Rev. B 80 (2009) 155441.
21. F. J. Culchac, R. B. Capaz, A. T. Costa and A. Latgé, *Magnetic response of zigzag nanoribbons under electric fields*, J. Phys.: Condens. Matter 26 (2014) 216002.
22. T. B. Prayitno, *Impossibility of increasing Néel temperature in zigzag graphene nanoribbon by electric field and carrier doping*, Physica E 129 (2021) 114641.
23. K. Sawada, F. Ishii and M. Saito, *Band-gap tuning in magnetic graphene nanoribbons*, Appl. Phys. Express 1 (2008) 064004.
24. H. Xie, J. -H. Gao and D. Han, *Excited spin density waves in zigzag graphene nanoribbons*, New J. Phys. 20 (2018) 013035.
25. C. Huang, H. Wu, K. Deng and E. Kan, *Edge-modified graphene nanoribbons: appearance of robust spiral magnetism*, J. Phys. Chem. C 121 (2017) 1371-1376.
26. J. T. Liang, X. H. Yan, Y. Zhang, Y. D. Guo and Y. Xiao, *Noncollinear magnetism in Lithium-doped zigzag graphene nanoribbons*, J. Magn. Magn.Mater. 480 (2019) 101-107.
27. T. B. Prayitno, *Electric-field-induced spin spiral state in bilayer zigzag graphene nanoribbons*, J. Phys.: Condens. Matter 33 (2021) 065805.
28. M. Y. Han, B. Özyilmaz, Y. Zhang and P. Kim, *Energy band-gap engineering of graphene nanoribbons*, Phys Rev Lett. 98 (2007) 206805.
29. X. Li, X. Wang, L. Zhang, S. Lee and H. Dai, *Chemically derived, ultra-smooth graphene nanoribbon semiconductors*. Science 319 (2008) 1229-1232.
30. L. Jiao, L. Zhang, X. Wang, G. Diankov and H. Dai, *Narrow graphene nanoribbons from carbon nanotubes*, Nature 458 (2009) 877-880.
31. J. B. Oostinga, H. B. Heersche, X. Liu, A. F. Morpurgo and L. M. K. Vandersypen, *Gate-induced insulating state in bilayer graphene devices*, Nat. Mater.7 (2008) 151-157.
32. B. N. Szafranek, D. Schall, M. Otto, D. Neumaier and H. Kurz, *Electrical observation of a tunable band gap in bilayer graphene nanoribbons at room temperature*, Appl. Phys. Lett. 96 (2010) 112103.
33. M. P. Lima, A. Fazzio and A. J. R. da Silva, *Edge effects in bilayer graphene nanoribbons: Ab initio total-energy density functional theory calculations*, Phys. Rev. B 79 (2009) 153401.
34. Y.-M. Lin and P. Avouris, *Strong suppression of electrical noise in bilayer graphene nanodevices*, Nano Lett. 8 (2008) 2119–2125.
35. X. Zhong, R. Pandey and S. P. Karna, *Stacking dependent electronic structure and transport in bilayer graphene nanoribbons*, Carbon 50 (2012) 784- 790.
36. A. Orlof, J. Ruseckas and I. V. Zozoulenko, *Effect of zigzag and armchair edges on the electronic transport in single-layer and bilayer graphene nanoribbons with defects*, Phys. Rev. B 88 (2013) 125409.
37. J. W. González, H. Santos, M. Pacheco, L. Chico and L. Brey, *Electronic transport through bilayer graphene flakes*, Phys. Rev. B 81 (2010) 195406.
38. E. Mostaani, N. D. Drummond and V. I. Fal'ko, *Quantum monte carlo calculation of the binding energy of bilayer graphene*, Phys. Rev. Lett. 115 (2015) 115501.
39. T. Asano and J. Nakamura, *Edge-state-induced stacking of zigzag graphene nanoribbons*, ACS Omega 4 (2019) 22035-22040.

40. K. Sawada, F. Ishii and M. Saito, *First-principles study of carrier-induced ferromagnetism in bilayer and multilayer zigzag graphene nanoribbons*, Appl. Phys. Lett. 104 (2014) 143111.
41. T. Ozaki, et al., *Open-source package for material explorer (OpenMX)*, http://www.openmx-square.org.
42. T. Ozaki and H. Kino, *Numerical atomic basis orbitals from H to Kr*, Phys.Rev. B 69 (2004) 195113.
43. N. Troullier and J. L. Martins, *Efficient pseudopotentials for plane-wave calculations*, Phys. Rev. B 43 (1991) 1993.
44. J. P. Perdew, K. Burke and M. Ernzerhof, *Generalized gradient approximation made simple*, Phys. Rev. Lett. 77 (1996) 3865.
45. H. Lee, N. Park, Y.-W. Son, S. Han and J. Yu, *Ferromagnetism at the edges of the stacked graphitic fragments: an ab initio study*, Chem. Phys. Lett. 398(2004) 207-211.
46. H. Lee, Y.-W. Son, N. Park, S. Han and J. Yu, *Magnetic ordering at the edges of graphitic fragments: Magnetic tail interactions between the edge- localized states*, Phys. Rev. B 72 (2005) 174431.
47. T. B. Prayitno, *Spin stiffness of bilayer zigzag graphene nanoribbon for several configurations*, Physica E 118 (2020) 113916.
48. K. Sawada, F. Ishii, M. Saito, S. Okada and T. Kawai, *Phase control of graphene nanoribbon by carrier doping: appearance of noncollinear magnetism*, Nano Lett. 9 (2009) 269–272.
49. T. B. Prayitno, *Controlling phase transition in monolayer metal diiodides XI_2 (X: Fe, Co, and Ni) by carrier doping*, J. Phys.: Condens. Matter 33 (2021) 335803.
50. L. Pan, J. An and Y.-J. Liu, *Noncollinear magnetism and half-metallicity in biased bilayer zigzag graphene nanoribbons*, New J. Phys. 15 (2013) 043016.